Enhanced long-term potentiation and impaired learning in mice with mutant postsynaptic density-95 protein

Martine Migaud*†, Paul Charlesworth*†, Maureen Dempster*†, Lorna C. Webster*†, Ayako M. Watabe‡, Michael Makhinson‡, Yong He§, Mark F. Ramsay†, Richard G. M. Morris†, John H. Morrison§, Thomas J. O'Dell‡ & Seth G. N. Grant*†

** Centre for Genome Research, and † Centre for Neuroscience, University of Edinburgh, Roger Land Building, West Mains Road, Edinburgh EH9 3JQ, UK*
‡ Department of Physiology and The Brain Research Institute, School of Medicine, University of California at Los Angeles, Los Angeles, California 90095, USA
§ Fishberg Research Centre for Neurobiology, Mount Sinai School of Medicine, Box 1065, One Gustave Levy Place, New York, New York 10029-6574, USA

Specific patterns of neuronal firing induce changes in synaptic strength that may contribute to learning and memory. If the postsynaptic NMDA (*N*-methyl-D-aspartate) receptors are blocked, long-term potentiation (LTP) and long-term depression (LTD) of synaptic transmission and the learning of spatial information are prevented. The NMDA receptor can bind a protein known as postsynaptic density-95 (PSD-95), which may regulate the localization of and/or signalling by the receptor. In mutant mice lacking PSD-95, the frequency function of NMDA-dependent LTP and LTD is shifted to produce strikingly enhanced LTP at different frequencies of synaptic stimulation. In keeping with neural-network models that incorporate bidirectional learning rules, this frequency shift is accompanied by severely impaired spatial learning. Synaptic NMDA-receptor currents, subunit expression, localization and synaptic morphology are all unaffected in the mutant mice. PSD-95 thus appears to be important in coupling the NMDA receptor to pathways that control bidirectional synaptic plasticity and learning.

In the mammalian hippocampus and other brain structures involved with memory formation, certain patterns of synaptic activity result in long-lasting modifications of the efficiency of synaptic transmission. In the CA1 region of the hippocampus, a train of low-frequency stimulation produces a reduction in synaptic efficacy (LTD) and high-frequency stimulation produces an increase (LTP)[1,2]. Mechanisms proposed to underlie these modifications of synaptic strength include changes in the sensitivity of postsynaptic transmitter receptors, activation of previously silent receptors, generation of retrograde messengers to the presynaptic terminal, structural changes in dendritic spines, and activation of transcription in the nucleus[1,2]. Although activation of the NMDA receptor initiates these complex events, its interactions with postsynaptic proteins and the signalling pathways immediately downstream from it are poorly understood.

The NMDA receptor is formed by the assembly of a common NR1 subunit with one or more of four different NR2 subunits, NR2A–D (refs 3, 4). The NR2 subunits have long cytoplasmic carboxy-terminal domains which contain sites for phosphorylation[5] and interaction with cytoplasmic proteins. *In vitro*, the C terminus of NR2 subunits binds to PSD-95/SAP90, chapsyn-110/PSD-93, and other related members of the membrane-associated guanylate kinase (MAGUK) family[6–9]. PSD-95/SAP90 (refs 10, 11) is an abundant postsynaptic density protein and contains several domains that participate in protein–protein interactions, including three PDZ/DHR (for PSD-95, Dlg, ZO-1/Dlg-homologous region) domains, an SH3 (Src-homology-3) domain and a guanylate kinase (GK)-homology domain. The second PDZ domain (PDZ2) can bind to the C terminus of the NR2 subunits[6,9]. PSD-95 has no detectable enzymatic activity and acts as an adapter molecule through protein–protein interactions mediated by the discrete domains. Although the function of PSD-95 at the synapse is unknown, in fibroblasts it mediates the localization of the NMDA receptor to focal clusters, indicating that PSD-95 may be required for the localization of such receptors to synapses[7].

To determine the function of PSD-95 in the brain, we characterized mice carrying a targeted mutation in the PSD-95 gene. Our results provide evidence that PSD-95 is important in signal transduction. NMDA-receptor-mediated synaptic plasticity was dramatically altered, with synapses becoming inappropriately strengthened after stimulation by a wide range of frequencies. The learning of PSD-95-mutant mice was impaired, supporting predictions of neural-network models that depend on bidirectional synaptic plasticity to mediate learning and memory.

PSD-95-mutant mice

The first two PDZ domains of PSD-95 bind to the NMDA-receptor subunits 2A (NR2A) and 2B (NR2B)[6,9], to K^+ channels[12] and to neuronal nitric oxide synthase[13] *in vitro*. We generated mice carrying a targeted mutation in the PSD-95 gene that leaves the first two PDZ domains intact by introducing a stop codon into the PDZ3 domain and replacing downstream sequences with an internal ribosome entry site that drives a β-galactosidase reporter gene (Fig. 1a). The targeting construct was electroporated into embryonic stem (ES) cells and Southern blot analysis indicated that homologous recombination had occurred in 5 clones out of 75 analysed (6.7%) (Fig. 1b). Three ES cell lines were microinjected into C57BL/6 blastocysts and two clones generated germline chimaeras, which were crossed onto the MF1 genetic background. No biochemical, anatomical, electrophysiological or behavioural differences were found between mice generated from two independent targeted clones. Heterozygous mice were intercrossed and the genetic status of the mice was determined by genomic Southern blotting and polymerase chain reaction (PCR) (Fig. 1b). From 70 litters, 602 mice were genotyped at weaning: 191 (32%) were wild type, 316 (52%) were heterozygotes, and 95 (16%) were homozygotes, demonstrating a distortion of the expected mendelian ratio ($\chi^2 = 32.1$, $P < 0.0001$). Runting was evident in 42% of viable homozygotes, which then recovered and reached the size of their wild-type littermates at ~6 weeks of age. Runting seemed to result from inadequate competition for feeding with wild-type siblings, because homozygous pups fostered to wild-type mothers were of normal size. Homozygous males and females were fertile and showed

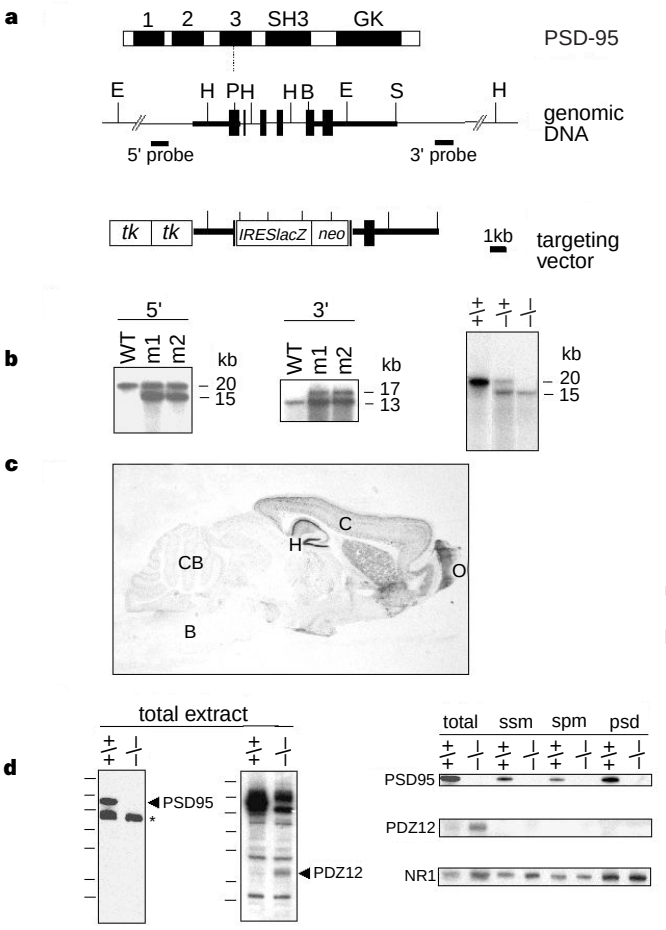

Figure 1 Targeted disruption of the PSD-95 gene. **a**, Top: PSD-95 protein with three PDZ domains (labelled 1, 2, 3), an Src homology 3 (SH3) domain and a guanylate kinase homology region (GK). Middle: PSD-95 gene with restriction-enzyme cutting sites (E, *Eco*RI; H, *Hin*dIII; P, *Pvu*II; B, *Bam*H1; S, *Sac*I); black boxes, exons, thick horizontal lines, homology regions used in the targeting vector; Southern blot probes are indicated. Bottom: targeting vector. *tk*, thymidine kinase gene; *IRES*, internal ribosome-entry sequence; *lacZ*, β-galactosidase gene; *neo*, neomycin-resistance gene. The dotted vertical line from the PDZ3 domain (upper) to the *Pvu*II site (middle) represents the position of the stop codon inserted into PDZ3. **b**, Left and centre, genomic Southern blot from ES cell clones (m1 and m2) digested with *Eco*RI and *Hin*dIII, hybridized with 5′ and 3′ probes, respectively. Right: genomic Southern blot of *Eco*RI-digested DNA from littermates of a heterozygote intercross and probed with the 5′ probe. Wild type (WT) (+/+), heterozygote (–/+) and homozygote (–/–) are indicated. **c**, Expression pattern of PSD-95 using X-gal-stained sagittal brain section. B, brainstem; H, hippocampus; C, cortex; CB, cerebellum; O, olfactory bulb. **d**, Immunoblots of PSD-95 protein in total forebrain extracts (left, middle panels) and in synaptosome subfractions (right panels) of wild-type mice (+/+) and PSD-95 mutants (–/–). Left: full-length PSD-95 in wild-type is indicated; asterisk, nonspecific band; size markers correspond to M_r 205K, 112K, 87K, 69K, 56K, 39K, 34K. Middle: the same blot was stripped and reprobed with an antibody recognizing PSD-95 N-terminal to the PDZ3 domain. The band labelled PDZ12 is found only in extracts of PSD-95 mutant mice and corresponds to the N-terminal domain expressed in the mutants. Right: extracts from synaptosome (ssm), synaptic plasma membrane (spm) and postsynaptic density (psd) fractions from wild-type and mutant mice immunoblotted with antibodies recognizing full-length PSD-95 (upper strip), N-terminal PDZ12 (middle strip) and NR1 (lower strip). The PSD-95^{PDZ12} (PDZ12) protein was not detected in spm or psd fractions even at very long exposures.

no sign of seizure, tremor or ataxia or of neurological abnormality. The expression of PSD-95 was shown by X-gal staining of brains of mutant mice (Fig. 1c) to be high in the forebrain, particularly in CA1 pyramidal neurons of the hippocampus and in granule cells in the dentate gyrus, in agreement with studies of messenger RNA *in situ*[6,13].

To determine the effects of mutating the PSD-95 protein we immunoblotted whole extracts from forebrain, synaptosomes, and synaptosome subfractions with antibodies raised against PSD-95 (Fig. 1d). Using three separate antibodies against PSD-95, a 95K band (corresponding to a relative molecular mass of 95,000) was detected for wild-type mice which was absent in homozygote mice. Immunoblotting with antibodies against the amino terminus of PSD-95 detected a 40K band in whole-brain extracts from homozygote mice, which corresponds to PDZ domains 1 and 2 and is now referred to as PSD-95^{PDZ12}. The PSD-95^{PDZ12} band was not detected in synaptosomes, in synaptic plasma membranes or in postsynaptic density fractions of homozygote mice, in contrast to full-length PSD-95 which was readily detectable in these fractions in wild-type mice (Fig. 1d). Control immunoblotting with antibodies specific for the NMDA R1 subunit (NR1) indicated that the distribution of NR1 in these fractions was the same as in wild-type mice. These results show that PSD-95^{PDZ12} does not localize to postsynaptic densities or to synaptic plasma membranes, but without a suitable antibody we cannot confirm this by immunohistochemistry. In PSD-95-mutant mice, no binding of PSD-95^{PDZ12} to the NMDA receptor could be detected by immunoprecipitation assay, although PSD-95 bound to the NMDA receptor from wild-type mice (data not shown). The amount of PSD-95^{PDZ12} found in PSD-95 mutants was ~10-fold less than full-length PSD-95 in wild-type, and as RNAse protection assays indicated that the level of mRNA in each was comparable (data not shown), the reason why we detected no interaction between PSD-95^{PDZ12} and the NMDA receptor is probably because PSD-95^{PDZ12} is not localized to synapses. This is consistent with data showing that the C-terminal domains of Dlg are required for membrane and subcellular localization[14].

Several other related neuronal MAGUK proteins have been described in addition to PSD-95, including chapsyn-110/PSD-93, SAP102 and SAP97 (refs 7, 8, 13, 15). The levels of these proteins were unaltered in our mutant mice (data not shown). We showed that chapsyn-110/PSD-93 could still interact with the NMDA receptor in PSD-95-mutant mice by immunoprecipitation and by immunoblotting the complex with antibodies against the NMDA receptor (data not shown). We conclude that the NMDA receptor in our PSD-95-mutant mice is bound by another MAGUK protein.

Synaptic localization of NMDA receptors

We next investigated the expression and localization of the NMDA receptor. The total amount of NR1, NR2A and NR2B proteins was the same in wild-type and mutant mice, and immunoprecipitation of each subunit and immunoblotting with the other subunits revealed no change in the composition of the receptor complexes (data not shown). These results indicate that PSD-95 is unlikely to play a role in regulating the stoichiometry of the NMDA-receptor subunit interaction *in vivo*. PSD-95 is highly expressed in the CA1 region of the hippocampus (Fig. 1c). Using light and electron microscopy, we found that the intensity of the Nissl staining pattern (data not shown) and the distribution of the dendritic marker MAP2 and of the synaptic-terminal marker synaptophysin were the same in the homozygous mutant and wild-type mice, indicating that the mutation does not affect cell density or cytoarchitectonic patterns (Fig. 2a–d). NR1 was widely distributed in soma and dendrites of CA1 in both mutant and wild-type mice and appeared similar in the light microscope (Fig. 2e, f). Electron microscopy revealed no changes in the morphology of these asymmetric synapses nor any difference in synapse density (Fig. 2i, j). Immunogold studies of NR1 in CA1 stratum radiatum detected no difference between the mutant and wild-type mice in the character-

istics or density of NR1 immunogold labelling of asymmetric synapses (Fig. 2g, h). In both sets of mice, NR1 was present primarily in the synaptic cleft and within the postsynaptic specialization, with minimal labelling in the neighbouring cytoplasm and no significant presynaptic labelling. Although these techniques are not quantitative, we found no major difference between mutant and wild-type mice in hippocampus CA1 synapse architecture or in NMDA-receptor localization. The localization of the NMDA receptor to the synapses of PSD-95 mutants by electron microscopy was confirmed by electrophysiological assay (see below).

NMDA-receptor function in mutant mice

We investigated the NMDA currents in primary cultured neurons derived from PSD-95-mutant and wild-type mice. Peak currents elicited by brief application of 250 μM NMDA/25 μM glycine in magnesium-free medium were not significantly different (3,907 ± 285 pA, $n = 36$ for PSD-95 mutant; 3,204 ± 328 pA, $n = 22$ for wild type; $t(56) = 1.578$, $P = 0.12$). Furthermore, the NMDA-receptor current–voltage relation did not change in PSD-95-mutant neurons in the presence and absence of magnesium (Fig. 3a, b). We investigated the synaptic expression of NMDA receptors in hippocampal slices using whole-cell voltage-clamp recordings to examine the NMDA-receptor-mediated component of excitatory postsynaptic currents (EPSCs) in CA1 pyramidal cells: we found no difference in the results from cells of wild-type and mutant animals (Fig. 3c). At a holding potential of −80 mV, where the NMDA-receptor ion channels are blocked by Mg^{2+}, EPSCs in CA1 pyramidal cells from wild-type animals ($n = 15$ cells from 4 animals) and PSD-95 mutants ($n = 18$ cells from 5 animals) have a similar ($t(7) = 0.49$; not significant), small NMDA-receptor-mediated component. The NMDA-receptor-mediated component of EPSCs from wild-type and PSD-95 mutant cells was also the same ($t(7) = 0.27$; not significant) at a holding potential of +40 mV, where the NMDA-receptor-mediated component of the EPSCs is larger owing to the relief of the Mg^{2+} block of the channel. These results show that NMDA-receptor channel properties are unaffected and that the receptors are normally localized to synapses in PSD-95-mutant mice. Moreover, field potential recordings showed that the maximal α-amino-3-hydroxy-5-methyl-4-isoxazole propionate (AMPA)-receptor-mediated field excitatory postsynaptic potential (fEPSP) amplitude evoked in wild-type and mutant slices was not significantly different (wild type: 8.6 ± 0.5 mV, $n = 69$ slices, 13 animals; PSD-95 mutant: 7.8 ± 0.4 mV, $n = 70$ slices, 15 animals), indicating that there is no gross disruption of synaptic transmission in our PSD-95-mutant mice.

We also compared paired-pulse facilitation, a short presynaptic form of synaptic plasticity, in the two sets of mice (Fig. 3d). We found that paired-pulse facilitation at inter-pulse intervals of 20, 50, 100 and 200 ms was significantly greater in slices from PSD-95-mutant mice ($P < 0.05$). As PSD-95 is thought to be a postsynaptic protein in forebrain synapses[16], this enhanced paired-pulse facilitation may be due to postsynaptic changes[17], or to retrograde signalling to the presynaptic terminal through PSD-95 interaction with neuroligin and neurexin[18] (as shown in Fig. 6a), or to some other effect such as an alteration in presynaptic K^+-channel function[19].

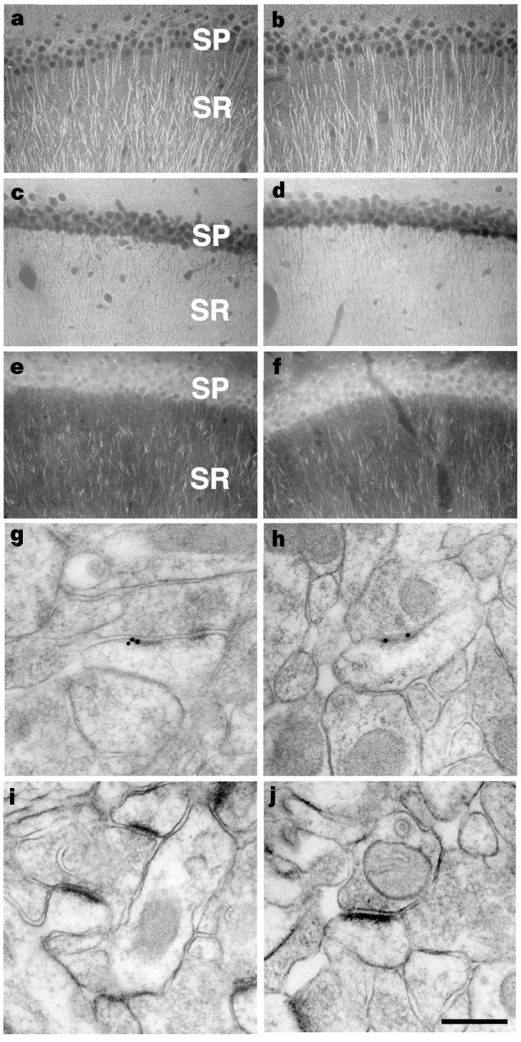

Figure 2 Anatomy and NR1 localization in hippocampus CA1 region of mice. **a**, **c**, **e**, **g**, **i**, Wild-type mice; **b**, **d**, **f**, **h**, **j**, PSD-95 mutant mice. **a**, **b**, MAP2 immunofluorescence; **c**, **d**, synaptophysin immunofluorescence; **e**, **f**, NR1 immunofluorescence; all photomicrographs are from a similar field of CA1, with the pyramidal cell layer (SP) at the top of the field, and the remaining two-thirds of the field occupied by the stratum radiatum (SR). **g**, **h**, Immunogold localization of NR1. Note that NR1 is localized at asymmetrical synapses in mutant and wild type mice. **i**, **j**, Standard morphology of the ultrastructure, with axospinous asymmetrical synapses shown in each case. Scale bar in **j** represents: for **a**–**f**, 70 μm; for **g**–**j**, 0.25 μm.

Synaptic plasticity in PSD-95 mutants

At many synapses in the brain, activation of postsynaptic NMDA receptors triggers complex multicomponent signalling pathways that can produce persistent changes in synaptic strength, such as LTP and LTD[1,2]. We therefore investigated whether PSD-95 might have a role in NMDA-receptor signalling by examining NMDA-receptor-dependent forms of synaptic plasticity in hippocampal slices from PSD-95-mutant mice. A conventional high-frequency stimulation protocol (100 Hz) that induces NMDA-receptor-dependent LTP produced a significantly larger potentiation of synaptic transmission in slices from PSD-95-mutant mice ($t(12) = 2.59$, $P < 0.025$; Fig. 4a). Immediately after high-frequency stimulation, the potentiation of synaptic transmission was similar in slices from wild-type and PSD-95-mutant mice; however, although synaptic strength remained at a steady-state potentiated level in wild-type slices (fEPSPs were potentiated to 193.6 ± 9.3% of baseline 60 min after high-frequency stimulation; $n = 7$), synaptic strength continued to grow over the next 30 min in slices from PSD-95-mutant mice (fEPSPs potentiated to 242.8 ± 17.5% of baseline; $n = 7$). To find the full extent of the enhanced LTP and the maximal LTP that could be generated in slices from PSD-95-mutant mice, we induced saturating levels of LTP with multiple trains of 100-Hz stimulation. As shown in Fig. 4b, LTP saturated at a much higher potentiated level in slices from mutant mice (298.4 ± 39.0% of baseline; $n = 5$) compared with wild-type slices (174.8 ± 14.0% of baseline; $n = 4$, $t(7) = 2.98$, $P < 0.05$).

We next quantified LTP induced by trains of low-frequency presynaptic stimulation. A 900-pulse train of 5-Hz stimulation, a near-threshold protocol for LTP induction[20], induced a small amount of LTP in slices from wild-type mice; fEPSPs were potentiated to

126.5 ± 7.3% of baseline after 45 min ($n = 7$) (Fig. 4c). In slices from PSD-95-mutant mice, synaptic transmission was potentiated to near saturation (fEPSPs were 278.4 ± 17.4% of baseline; $n = 6$) (Fig. 4c). The NMDA-receptor antagonist 2-amino-5-phosphonovaleric acid (AP5) blocked 5-Hz-stimulation-induced LTP in both wild-type and PSD-95-mutant mice (fEPSPs in slices from PSD-95-mutant mice were 110.2 ± 11.7% of baseline ($n = 5$) in 100 μM D,L-AP5 and 98.5 ± 3.4% of baseline in slices from wild-type mice ($n = 5$)), indicating that the enhanced LTP in slices from PSD-95-mutant mice is not due to upregulation of NMDA-receptor-independent

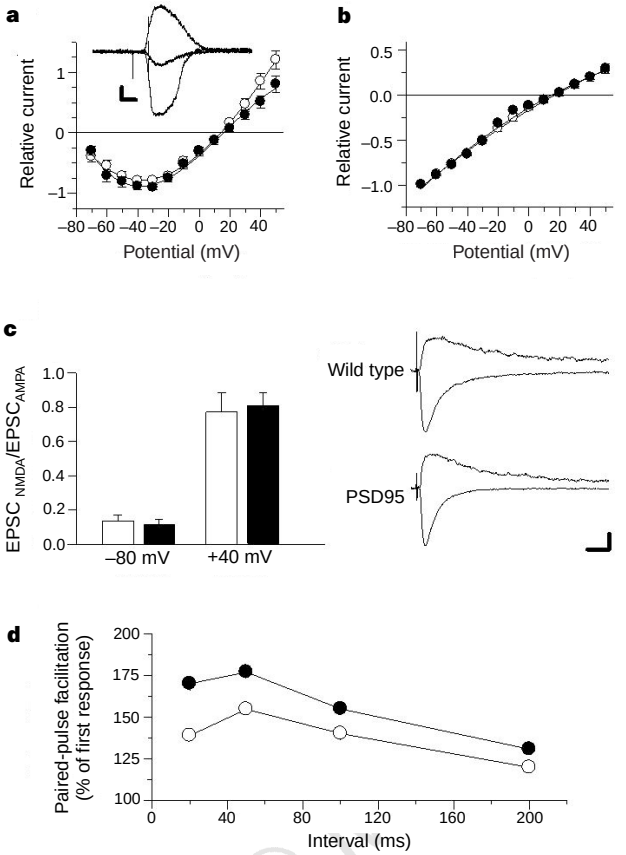

Figure 3 NMDA-receptor currents and synaptic physiology. **a**, Current–voltage relationship for NMDA (250 μM)-receptor-gated currents recorded in the presence of magnesium (1 mM) (white circles, wild type ($n = 10$); filled circles, PSD-95 mutant ($n = 16$)). Insert, currents recorded from a single PSD-95 mutant cell at –70 mV (middle trace), –20 mV (lower trace), and +50 mV (upper trace). Calibration bars are 50 ms and 100 pA. **b**, Current–voltage relationship for NMDA (250 μM)-receptor-gated currents recorded in magnesium-free solution (white circles, wild type ($n = 12$); filled circles, PSD-95 mutant ($n = 24$)). **c**, Synaptic NMDA-receptor currents. The bars show the magnitude of the NMDA-receptor-mediated component EPSCs (normalized to the magnitude of the AMPA-receptor-mediated component; see Methods). At postsynaptic holding potentials of both –80 mV and +40 mV, the NMDA-receptor-mediated component of the EPSCs in CA1 pyramidal cells from PSD-95 mutants (black bars) is indistinguishable from that seen in pyramidal cells from wild-type animals (white bars). Traces show representative EPSCs elicited in a wild-type cell (top) and a PSD-95-mutant cell (bottom) at +40 mV (outward-going currents) and –80 mV (inward-going currents). Each trace is the average of four EPSCs elicited at each holding potential. Calibration bars indicate 20 ms and 50 pA. **d**, Paired-pulse facilitation of fEPSPs was measured using pairs of presynaptic fibre stimulation pulses separated by 20, 50, 100 and 200 ms. Note the larger facilitation ($P < 0.05$) seen in slices from PSD-95-mutant animals (filled symbols) compared to wild type (open symbols). Each point is the mean ± s.e.m. (error bars are smaller than point used to plot the mean value).

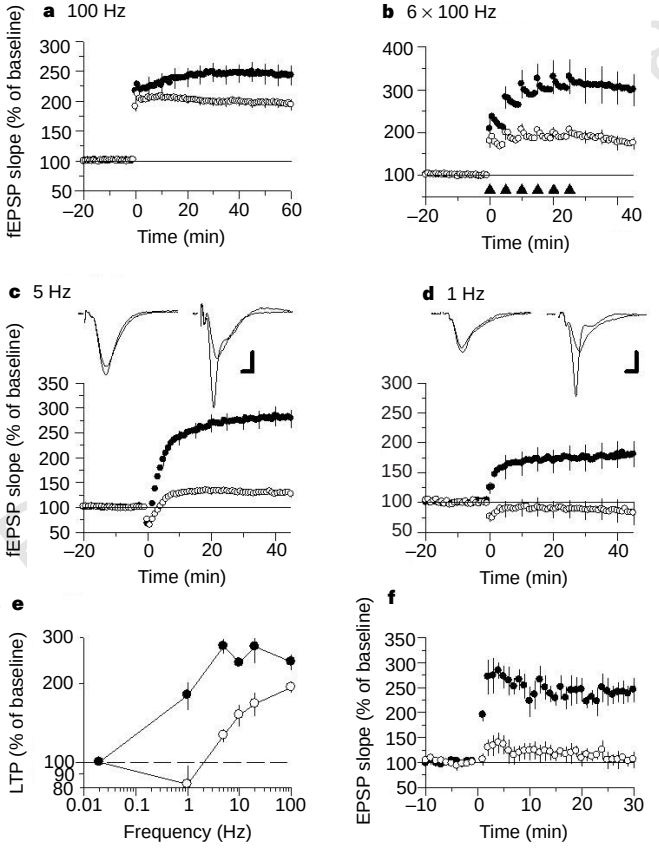

Figure 4 Frequency-dependent changes in synaptic strength. **a**, High-frequency stimulation-induced LTP was elicited using two trains of 100-Hz stimulation delivered at time zero. Note the larger potentiation seen 60 min after 100-Hz stimulation in slices from PSD-95 mutant animals (black symbols) compared with slices from wild-type animals (white symbols). **b**, Single 1-s trains of 100-Hz stimulation were delivered six times (at points indicated by black triangles) starting at time zero. Synaptic transmission in wild-type slices (white symbols) shows no further increase after the second train; transmission in slices for PSD-95 mutants continues to increase and saturates at a much higher level. **c**, **d**, 900 stimulation pulses were delivered at time zero at either 5 Hz (**c**) or 1 Hz (**d**). Although these stimulation protocols produce small amounts of either LTP (5 Hz) or LTD (1 Hz) in slices from wild-type animals (white symbols), both stimulation protocols induce large LTP in slices from PSD-95 mutant animals (black symbols). The fEPSPs in **c** were recorded during baseline and 45 min after 5-Hz stimulation in wild-type (left) and PSD-95 mutant animals (right). The fEPSPs in **d** were recorded before and 45 min after 1-Hz stimulation in slices from wild-type (left, smaller response is after 1-Hz stimulation) and PSD-95 mutant animals (right, larger response is after 1-Hz stimulation). Calibration bars in **c** and **d** indicate 2 mV and 2 ms. **e**, Summary of the ability of different frequencies of synaptic stimulation to induce persistent changes in synaptic strength in hippocampal slices from wild-type (white symbols) or PSD-95 mutant (black symbols) animals; 0.02 Hz, which corresponds to the stimulation frequency used to monitor synaptic transmission throughout the experiments, had no effect on synaptic transmission in slices from wild-type and PSD-95 mutant animals. The line at 100% of baseline corresponds to no lasting change in synaptic strength. **f**, EPSPs evoked once every 30 s were recorded intracellularly from individual CA1 pyramidal cells. Following 10 min of baseline recording, 30 EPSPs (evoked at 0.5 Hz) were each paired with a 150-ms, 1.0-nA depolarizing current pulse delivered through the recording electrode starting 10 ms after the start of an EPSP. Data are from 12 wild-type cells ($n = 4$ animals; white symbols) and 11 PSD-95 mutant cells ($n = 4$ animals; black symbols).

forms of LTP. A large enhancement of LTP in PSD-95-mutant slices was also stimulated by intermediate frequencies. In wild-type slices, 900 pulses of 10 and 20 Hz induced potentiations of 151.6 ± 14.8% ($n = 4$) and 167.4 ± 17.7% of baseline ($n = 6$), respectively, whereas fEPSPs from PSD-95-mutant mice were potentiated to 240.2 ± 4.6% ($n = 5$) and 277.3 ± 37.5% ($n = 6$) of baseline, respectively. Finally, we used a low-frequency protocol (1 Hz, 900 pulses) that induces LTD in hippocampal slices[21] from young wild-type mice and induces a small and nonsignificant depression of synaptic transmission in slices from adult wild-type mice (fEPSPs were 82.2 ± 19.6% of baseline ($n = 4$, $t(3) = 0.91$), compared with pre-1 Hz baseline) (Fig. 4d). In response to this stimulation protocol, slices from adult PSD-95-mutant mice showed a significant LTP (fEPSPs were 180.4 ± 21.8% of baseline; $n = 5$, $t(4) = 3.69$, $P < 0.025$) (Fig. 4d). As summarized in Fig. 4e, these results indicate that the frequency sensitivity of LTP induction in the CA1 region of the hippocampus is altered in PSD-95-mutant mice.

To determine whether the enhanced LTP was due to altered inhibitory synaptic transmission, we tested potentiation in the presence of GABA inhibitors. Although 50 pulses of stimulation at 2.5 Hz elicited little LTP in slices from wild-type mice (fEPSPs were potentiated to 126.5 ± 8.3% of baseline; $n = 7$), we found that synaptic transmission was potentiated to 232.76 ± 30.4% of baseline in slices from PSD-95-mutant mice ($n = 3$, $t(8) = 4.93$, $P < 0.005$, compared to wild-type). When inhibitory synaptic transmission was blocked by 50–100 μM picrotoxin, 50 pulses of 2.5 Hz still elicited a significantly ($t(4) = 2.99$, $P < 0.025$) larger LTP in slices from PSD-95-mutant mice (fEPSPs were potentiated to 271.9 ± 31.1% ($n = 3$) of baseline in slices from PSD-95 mutants, and 175.6 ± 8.3% ($n = 3$) of baseline in slices from wild-type mice). In addition, when inhibitory synaptic transmission was blocked by 100 μM picrotoxin and intracellular microelectrodes were used to record EPSPs, we found that pairing low-frequency presynaptic fibre stimulation (0.5 Hz) with postsynaptic depolarization induced significantly larger LTP in cells from PSD-95 mutants (30 min post-pairing EPSPs were 105 ± 11.8% of baseline in wild-type cells and 245 ± 25.1% of baseline in PSD-95 mutant cells; $t(6) = 4.64$, $P < 0.005$; Fig. 4f). Therefore, the enhanced induction of LTP in PSD-95 mutants does not seem to arise from alterations in inhibitory synaptic transmission. Moreover, the larger potentiation induced by pairing low-frequency presynaptic fibre stimulation with postsynaptic depolarization in PSD-95 mutants indicates that changes in paired-pulse facilitation or postsynaptic excitability are unlikely to underlie the LTP enhancement seen in PSD-95 mutants.

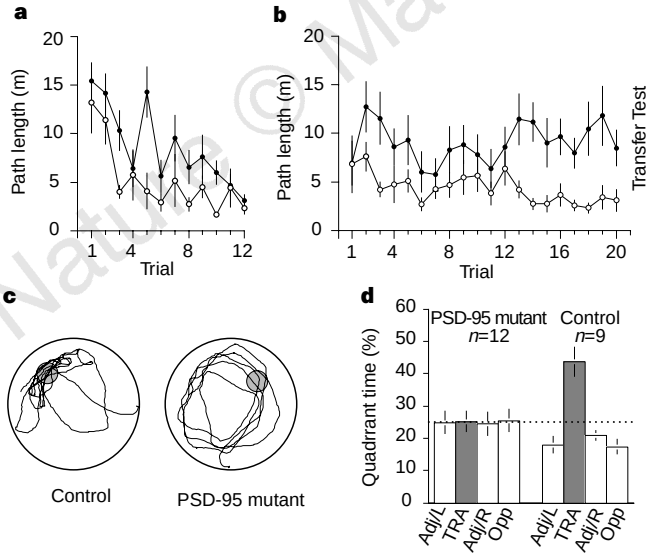

Figure 5 Behavioural data. **a**, Path length across 3 days of training to a visible cue (4 trials per day). By trial 12, the path lengths of both groups in the 2-m-diameter pool were equivalent and close to the minimum possible. Control, white symbols; PSD-95, filled symbols (mean ± 1 s.e.m.). **b**, Path length across 5 days of place-learning to a hidden platform. Wild-type controls learn to take relatively direct paths, whereas PSD-mutant mice persist in taking circuitous routes. **c**, **d**, Representative swim paths (**c**) and per cent time spent in each quadrant (**d**) during the 60-s transfer test in which the hidden platform (grey in **c**) is not present in the pool. Wild-type mice consistently search in the correct location but PSD-95 mutant mice swim all over the pool. Further training (for up to 32 trials) failed to reveal spatial learning in PSD-95 mutant mice (see text). The horizontal dotted line at 25% in **d** indicates chance performance. Training quadrant, TRA; adjacent left, Adj/L; adjacent right, Adj/R; opposite, Opp.

Learning and memory in PSD-95 mutants

Neural-network models of learning and memory incorporating bidirectional synaptic plasticity (LTP and LTD) predict that major alterations in the frequency function should be deleterious to learning. We therefore tested spatial learning in a watermaze, which is dependent on hippocampus NMDA-receptor function[22,23]. Adult littermate wild-type ($n = 9$) and homozygous ($n = 12$) mice swam in the pool and mounted the platform in the normal ways. With the experimenter blind with respect to genotype, we monitored the animals as they learned to approach a platform marked with a visible cue (Fig. 5a). Both wild-type and PSD-95 mutants reduced the length of their path across the training period (Fig. 5a). Although the mutant mice were initially slower, no difference between groups was seen over the last 6 trials ($P < 0.05$). We then tested spatial learning using the hidden platform version of the watermaze. The mutant mice had significantly longer swim paths than wild-type mice (controls, 4.32 ± 0.30 m; PSD-95 mutants, 9.04 ± 0.50 m; $F(1, 19) = 5.66$, $P < 0.05$; Fig. 5b). After 20 training trials, performance in a transfer test (with the platform removed) was used as an index of learning (Fig. 5c, d). Wild-type mice showed a spatial bias towards the training quadrant, spending significantly more time searching there than in the other three quadrants ($F(3, 24) = 13.84$; $P < 0.0001$), unlike the mutant mice ($F < 1$, $P < 0.9$; group by quadrant interaction, $F(3, 57) = 5.41$; $P < 0.005$). The mice were then given further training using a smaller platform until they reached a specified criterion, or until 32 trials had been completed. All controls (9/9) reached this criterion in 15.1 ± 2.4 trials whereas only 2/12 PSD-95 mutants were successful, giving a group mean of 29.3 ± 2.0 trials ($F(1, 9) = 20.51$; $P < 0.0005$). The PSD-95-mutant mice therefore had a marked inability to learn the position of the hidden platform, an effect also seen when NMDA receptors are blocked[22,23].

Discussion

PSD-95 has been suggested in *in vitro* studies[7] to localize NMDA receptors to the synapse and our results show that they are synaptically localized in PSD-95-mutant mice. This raises the possibility that other molecules may be more important in localizing NMDA-receptor subunits to the synapse. Receptor localization could be achieved by actin in dendritic spines[24]; actin may interact with NMDA-receptor subunits through α-actinin[25] and spectrin[26]. The NMDA receptor may experience two sets of interactions: one controlling receptor localization and turnover, which is independent of PSD-95, and a second operating through PSD-95 on signal-transduction pathways that control synaptic strength (Fig. 6a).

A wide range of frequencies and patterns of pre- and postsynaptic activity probably act through NMDA-receptor-dependent forms of synaptic plasticity to modulate dynamically the strength of excitatory synaptic transmission *in vivo*. In our PSD-95-mutant mice, the frequency-response function controlling the induction of persistent changes in synaptic efficacy[24] showed a dramatic leftward and upward shift so that all frequencies tested (1, 5, 10, 20, 100 Hz) induced LTP. This propensity towards potentiation was most marked at low frequencies, where for example 1-Hz stimulation produced no potentiation in wild-type mice but a large LTP in the PSD-95 mutants. This enhanced LTP requires the activation of NMDA receptors and reaches the enhanced level during the first

30 min after high-frequency stimulation (100 Hz). Postsynaptic kinases and phosphatases are known to regulate long-term plasticity during this time window[1,2], which suggests that a pathway downstream from the NMDA receptor has been modified in the PSD-95 mutants. Components of this pathway could include PSD-95-binding proteins such as SynGAP[28,29], neuroligin[18], GKAP/SAPAP[30,31], neuronal NO synthase[13] and postsynaptic phosphatases that participate in LTD. A model of the NMDA receptor, PSD-95 and associated proteins in a signal-transduction complex (Fig. 6a) in which the associated proteins participate in downstream signalling is in keeping with the 'transducisome' model described for *Drosophila*, where the Trp calcium channel binds PDZ-domain-containing proteins that mediate assembly of a signalling complex[32]. One function of this complex that is suggested by our paired-pulse facilitation data is to allow the postsynaptic NMDA receptor to regulate transmitter release as a result of PSD-95/neuroligan/neurexin interaction with the presynaptic terminal.

Mathematical models of synaptic plasticity that include bidirectional modifications of synaptic strength (potentiation and depression)[27,33] when incorporated into neural-network simulations have implications that bear on our PSD-95-mutant mice (Fig. 6b, c). Unlike networks composed of synapses exhibiting only potentiation of synaptic strength, bidirectionally modifiable synapses can increase storage capacity, reduce errors, and limit the number and strength of potentiated synapses to an optimum for memory storage[34,35]. Hippocampal neurons fire in the θ range of 4–12 Hz during exploratory behaviour[36], and in this range neurons in PSD-95 mutants show dramatic LTP, unlike neurons in wild-type mice which are near the threshold between LTP and LTD. Consequently, training of PSD-95-mutant mice in a spatial learning task might cause too many synapses within the network to become strongly potentiated and not enough to be depressed, resulting in a degradation of information storage and recall capacity, which manifests as a learning impairment. Genetic manipulation of PSD-95 will enable bidirectional regulation of synaptic strength to be controlled and provide further insight into synaptic plasticity and neural networks and their integrated function in learning and memory. □

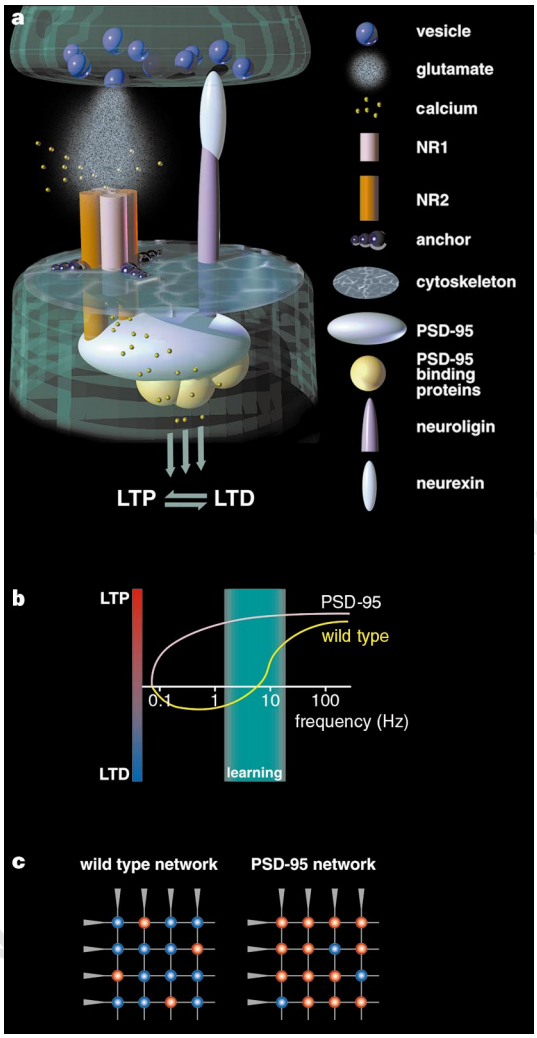

Figure 6 Model for PSD-95 function. **a**, The NMDA-receptor/PSD-95 complex at the synapse with presynaptic terminal with synaptic vesicles (top) and dendritic spine (bottom). NR2 subunits bind PSD-95, which binds neuronal NO synthase, SynGAP, GKAP/SAPAP proteins and neuroligin, which binds the presynaptic protein neurexin. Anchoring proteins tether the transduction complex through NMDA-receptor subunits to the postsynaptic cytoskeleton. Glutamate release from the presynaptic terminal leads to Ca^{2+} influx, which together with PSD-95 and associated proteins may regulate the balance between LTP and LTD (arrows). **b**, **c**, A model to explain the learning defects in PSD-95 mutant mice, based on learning rules using bidirectional synaptic plasticity. **b**, Postsynaptic activity (as a function of the frequency of trains of synaptic stimulation in Hz) is plotted against the corresponding degree of LTP (red) and LTD (blue). The green box (labelled learning) shows the firing frequency of hippocampal CA1 neurons during exploratory behaviour: in this range, synapses in wild-type mice may show either LTP or LTD, whereas PSD-95 mutant synapses are more likely to show LTP. **c**, This is indicated in a neural network in which PSD-95 mutants have an inappropriately higher number of synapses showing LTP (red) and too few showing LTD (blue). Grey triangles are cell bodies, and processes are lines that intersect as synapses; the colour (blue–red) indicates the strength of synaptic transmission.

Methods

Gene targeting and biochemistry. The targeting vector comprised 1.6-kb and 4.2-kb bands of, respectively, 5′ and 3′ genomic DNA flanking a cassette (TAG3IRES1acZpA-MC1neopA) containing the positive selectable marker MC1-neo (neomycin). The 5′ end of this cassette contained stop codons in all reading frames to terminate translation of PSD-95 at the *Pvu*II site in PDZ3, followed by an internal ribosome-entry site (IRES) which allows a β-galactosidase reporter gene to be expressed under the control of PSD-95. For negative selection, two copies of the thymidine kinase gene (MC1-tk) was ligated 5′ to the 5′ homology arm. The targeting construct was linearized and electroporated into ES cells (E14Tg2αIV clone). For Southern blot analysis, 5–15 μg DNA from ES cells or tail tips were digested with *Eco*RI or *Hin*dIII and probed with a 0.8-kb cDNA fragment (5′ probe) or a 1.2-kb genomic DNA (3′ probe) flanking the homology region. Genotyping using PCR required two independent reactions. The wild-type allele was amplified (220-bp product) using a forward primer upstream of the *Pvu*II site in the PDZ3 domain (AACCAAGGCGGATCGTGATCCA) and a reverse primer (TCTCTTTGGTGGGCAGTG). The mutant allele (2-kb product) was amplified using a forward primer in the *neo* gene (CATTCGACCACCAAGCG AAAGATC) and a reverse primer (CAGGGAGCGGGGACGGATGA) in PSD-95. Amplification was for 30 cycles of 30 s at 93 °C, 60 s at 55 °C, 60 s at 72 °C. Standard procedures were used for synaptosome preparation, protein extraction, immunoblotting and immunoprecipitation. Antibodies: against NR1, mAb 54.1 and pAb 1516 (Chemicon); against PSD-95, pAb138, raised against the N-terminal 438 residues of a mouse PSD-95 fusion protein, and mAb PSD-95 (Transduction Labs).

Neuroanatomy. All procedures relating to the care and treatment of mice conformed with institutional and NIH guidelines. Nine mice were anaesthetized with a lethal dose of chloral hydrate and perfused with aldehydes, dissected, post-fixed, and sectioned[37]. 50-μm vibratome sections were used for immunohistochemistry and 15-μm freshly frozen sections were used for X-gal (5-bromo-4-chloro-3-indolyl-β-galactoside) (Nova Biochem) staining. Primary antibodies were: anti-NR1 mAb 54.1 (1/100); anti-synaptophysin mAb SY38 (1/10; Boehringer); non-phosphorylated neurofilament mAb SMI32 (1/7,500; Steinburger Monoclonal); MAP2 mAb HM2 (1/800; Sigma Immuno Chemicals). Standard procedures were followed for immunofluorescent staining, mounting and coverslipping[37]. Sections were examined and photographed by experimenters blind to genotype. For post-embedding immunogold localization, six additional mice were perfused with a fixative composed of 2.5% glutaraldehyde, 1% paraformaldehyde and 0.1% picric acid in 0.1M PBS, pH

7.3. After fixation, vibratome sections of CA1 were collected, embedded in resin, thin-sectioned, prepared for post-embedding immunogold localization of NR1, and viewed at 60 kV on a Zeiss CH-10 electron microscope, as described[37]. Control experiments in which grids were incubated in buffer instead of the NR1 antibody showed no immunogold labelling.

Electrophysiology. 400-μm-thick slices of mouse hippocampus were maintained at 30 °C in an interface-type recording chamber perfused with a murine artificial cerebrospinal fluid (ACSF) containing 124 mM NaCl, 4.4 mM KCl, 25 mM Na_2HCO_3, 1 mM NaH_2PO_4, 1.2 $MgSO_4$, 2 mM $CaCl_2$ and 10 mM glucose. fEPSPs elicited by Schaffer collateral/commissural fibre stimulation were recorded in the CA1 region as described[20]. Glass microelectrodes filled with 2 M CsCl (resistance, 60–140 MOhms) were used to record EPSPs from individual CA1 pyramidal cells and current injected through the recording electrode was used to hyperpolarize cells to between −90 and −95 mV. There were no differences between mutant and wild-type cells in either resting membrane potential or input resistance. In these experiments, slices with the CA3 region removed were bathed in a modified, 100 μM picrotoxin-containing ACSF in which the concentrations of $CaCl_2$ and $MgSO_4$ were raised to 4.0 mM each and the concentration of KCl was reduced to 2.4 mM. High-frequency-stimulated LTP was induced using 2-s and 1-s trains of 100-Hz stimulation (intertrain interval was 10 s). Saturating levels of LTP were induced by six deliveries of single 1-s trains of 100-Hz stimulation every 5 min. To test synaptic responses mediated by NMDA receptors in mutant and wild-type mice, we used whole-cell voltage-clamp techniques to record EPSCs due to Schaffer collateral fibre stimulation in CA1 pyramidal cells held at membrane potentials between −80 and +40 mV. Low-resistance (3–5 MΩ; access resistances ranged from 12.5 to 27 MΩ) patch-clamp electrodes were filled with a solution containing 140 mM CsCl, 1 mM $MgCl_2$, 0.2 mM EGTA, 2 mM Mg-ATP, 0.3 mM GTP and 10 mM HEPES, pH 7.2. In some experiments, electrodes were filled with a solution containing 122.5 mM caesium gluconate, 15 mM CsCl, 2.5 mM TEA-Cl, 1.4 mM NaCl, 0.2 mM EGTA, 2 mM Mg-ATP, 0.3 mM GTP and 10 HEPES, pH 7.2. In these experiments, slices with the CA3 region removed were maintained at room temperature (20 to 22 °C) in a submerged recording chamber perfused (2–3 ml per min) with a modified ACSF containing 100 μM picrotoxin, 2.4 mM KCl, and double the normal concentrations of $CaCl_2$ and $MgSO_4$. The AMPA- and NMDA-receptor-mediated components of the EPSCs were estimated from the amplitude of the synaptic currents measured at 5 and 50 ms after the start of the EPSC, respectively. To compare across cells the size of the NMDA-receptor-mediated component of the EPSC, it was normalized to the size of the AMPA-receptor-mediated component. All values are reported as mean ± s.e.m., n being the number of mice. All experiments were performed blind, and after data collection the genotypes were revealed for analysis. Primary cultures of forebrain neurons were prepared from individual neonatal mice (P1) as described[38]. Whole-cell patch-clamp recordings were made from cells cultured for 12–20 days (wild type, mean age of 13.6 d; PSD-95 mutant, mean age of 16.3 d), which was after the age at which PSD-95 expression was observed by using X-gal staining. The composition of the recording electrode solution was (in mM): $CsMeSO_3$ 100, Cs-BAPTA 5, HEPES 15, Mg-ATP 4, Na-GTP 0.4, sucrose 40, adjusted to pH 7.2 with CsOH. The composition of the bathing medium was (in mM): NaCl 140, KCl 3, $CaCl_2$ 2.5, HEPES 15, glucose 10, $MgCl_2$ 0 or 1, adjusted to pH 7.4 with NaOH. Currents were evoked by brief (50-ms) application of 250 μM NMDA + 25 μM glycine. The calculated junction potential of +15 mV was not corrected for in the data shown here. Student t-tests were used to assess statistical significance.

Behavioural testing. We used an open-field watermaze (2 m in diameter, opaque water, 25 ± 1 °C, automated swim-path monitoring). Visible platform training: mice were trained to a randomly located platform with a striped flag protruding above it (4 trials per day for 3 days; 30-cm-diameter platform; curtains drawn around the pool to occlude extra-maze cues; maximum trial duration was 90 s; intertrial interval (ITI), 10 min). Hidden platform training: we used a hidden platform with the extra-maze cues visible (4 trials per day, 5 days, 30-cm platform; platform area/pool area was 1/44; 30 s was spent on the platform at the end of each trial; ITI, 10 min). Transfer test: 10 min after the previous training trial, mice were placed in the pool for 60 s (platform absent; the start position was opposite to whatever training quadrant had bene used for an individual animal). Training to criterion: extended hidden-platform training, using a smaller hidden platform (20 cm diameter; platform area/pool area was 1/100) until the animals completed 2 consecutive days with each trial of <20 s, or until 32 trials had been done.

Received 9 June; accepted 13 October 1998.

1. Bear, M. F. & Malenka, R. C. Synaptic plasticity: LTP and LTD. *Curr. Opin. Neurobiol.* **4,** 389–399 (1994).
2. Bliss, T. V. P. & Collingridge, G. L. A synaptic model of memory: long-term potentiation in the hippocampus. *Nature* **361,** 31–39 (1993).
3. Hollman, M. & Heinemann, S. Cloned glutamate receptors. *Annu. Rev. Neurosci.* **17,** 31–108 (1994).
4. Nakanishi, S. & Masu, M. Molecular diversity and functions of glutamate receptors. *Annu. Rev. Biophys. Biomolec. Struct.* **23,** 314–348 (1994).
5. Smart, T. G. Regulation of excitatory and inhibitory neurotransmitter-gated ion channels by protein phosphorylation. *Curr. Opin. Neurobiol.* **7,** 358–367 (1997).
6. Kornau, H.-C., Schenker, L. T., Kennedy, M. B. & Seeburg, P. H. Domain interaction between NMDA receptor subunits and the postsynaptic density protein PSD-95. *Science* **269,** 1737–1740 (1995).
7. Kim, E., Cho, K.-O., Rothschild, A. & Sheng, M. Heteromultimeriozation and NMDA receptor-clustering activity of chapsyn-110, a member of the PSD-95 family of proteins. *Neuron* **17,** 103–113 (1996).
8. Müller, B. M. *et al.* SAP102, a novel postsynaptic protein that interacts with NMDA receptor complexes *in vivo*. *Neuron* **17,** 255–265 (1996).
9. Niethammer, M., Kim, E. & Sheng, M. Interaction between the C terminus of NMDA receptor subunits and mutliple members of the PSD-95 family of membrane-associated guanylate kinases. *J. Neurosci.* **16,** 2157–2163 (1996).
10. Cho, K. O., Hunt, C. A. & Kennedy, M. B. The rat brain postsynaptic density fraction contains a homolog of the *Drosophila* discs-large tumor suppressor protein. *Neuron* **9,** 929–942 (1992).
11. Kistner, U. *et al.* SAP90, a rat presynaptic protein related to the product of the *Drosophila* tumor suppressor gene *dlg-A*. *J. Biol. Chem.* **268,** 4580–4583 (1993).
12. Kim, E., Niethammer, M., Rothschild, A., Jan, Y. N. & Sheng, M. Clustering of shaker-type K^+ channels by interaction with a family of membrane-associated guanylate kinases. *Nature* **378,** 85–88 (1995).
13. Brenman, J. E. *et al.* Interaction of nitric oxide synthase with the postsynaptic density protein PSD–95 and alpha1-syntrophin mediated by PDZ domains. *Cell* **84,** 757–767 (1996).
14. Hough, C. D., Woods, D. F., Park, S. & Bryant, P. J. Organizing a functional junctional complex requires specific domains of the *Drosophila* MAGUK discs-large. *Genes Dev.* **11,** 3242–3252 (1997).
15. Müller, B. M. *et al.* Molecular characterization and spatial distribution of SAP97, a novel presynaptic protein homologous to SAP90 and the *Drosophila* discs-large tumor suppressor protein. *J. Neurosci.* **15,** 2354–2366 (1995).
16. Hunt, C. A., Schenker, L. J. & Kennedy, M. B. PSD-95 is associated with the postsynaptic density and not with the presynaptic membrane in forebrain synapses. *J. Neurosci.* **16,** 1380–1388 (1996).
17. Wang, J. H. & Kelly, P. A. T. Attenuation of paired-pulse facilitation associated with synaptic potentiation mediated by postsynaptic mechanisms. *J. Neurophysiol.* **78,** 2707–2716 (1997).
18. Irie, M. *et al.* Binding of neuroligins to PSD-95. *Science* **277,** 1511–1515 (1997).
19. Tejedor, F. J. *et al.* Essential role for dlg in synaptic clustering of shaker K^+ channels *in vivo*. *J. Neurosci.* **17,** 152–159 (1997).
20. Mayford, M., Wang, J., Kandel, E. R. & O'Dell, T. J. CaMKII regulates the frequency-response function of hipocampal synapses for the production of both LTD and LTP. *Cell* **81,** 891–904 (1995).
21. Dudek, S. M. & Bear, M. F. Bidirectional long-term modification of synaptic effectiveness in the adult and immature hippocampus. *J. Neurosci.* **13,** 2910–2918 (1993).
22. Morris, R. G. M., Anderson, E., Lynch, G. S. & Baudry, M. Selective impairment of learning and blockade of long-term potentiation by an *N*-methyl-D-aspartate receptor antagonist, AP5. *Nature* **319,** 774–776 (1986).
23. Tsien, J. Z., Huerta, P. T. & Tonegawa, S. The essential role of hippocampal CA1 NMDA receptor-dependent synaptic plasticity in spatial memory. *Cell* **87,** 1327–1338 (1996).
24. Allison, D. W., Gelfand, V. I., Spector, I. & Craig, A. M. Role of actin in anchoring postsynaptic receptors in cultured hippocampal neurons: Differential attachment of NMDA versus AMPA receptors. *J. Neurosci.* **18,** 2423–2436 (1998).
25. Wyszynski, M. *et al.* Competitive binding of α-actinin and calmodulin to the NMDA receptor. *Nature* **385,** 439–442 (1997).
26. Wechsler, A. & Teichberg, V. I. Brain spectrin binding to the NMDA receptor is regulated by phosphorylation, calcium and calmodulin. *EMBO J.* **17,** 3931–3939 (1998).
27. Bienenstock, E., Cooper, L. & Munro, P. Theory for the development of neuron selectivity: orientation specificity and binocular interaction in visual cortex. *J. Neurosci.* **2,** 32–48 (1982).
28. Kim, J. H., Liao, D., Lau, L.-F. & Huganir, R. SynGAP: a synaptic RasGAP that associates with the PSD-95/SAP90 protein family. *Neuron* **20,** 683–691 (1998).
29. Chen, H.-J., Rojas-Soto, M., Oguni, A. & Kennedy, M. B. A synaptic Ras GTPase-activating protein (p135 SynGAP) inhibited by CaM kinase II. *Neuron* **20,** 895–904 (1998).
30. Naisbitt, S. *et al.* Characterization of guanylate kinase-associated protein, a postsynaptic density protein at excitatory synapses that interacts directly with postsynaptic density-95/synapse-associated protein 90. *J. Neurosci.* **17,** 5687–5696 (1997).
31. Takeuchi, M. *et al.* SAPAPs: A family of PSD-95/SAP90-associated proteins localized at postsynaptic density. *J. Biol. Chem.* **272,** 11943–11951 (1997).
32. Tsunoda, S. *et al.* A multivalent PDZ-domain protein assembles signalling complexes in a G-protein-coupled cascade. *Nature* **388,** 243–249 (1997).
33. Sejnowski, T. J. Statistical constraints on synaptic plasticity. *J. Theor. Biol.* **69,** 387–389 (1977).
34. Willshaw, D. & Dayan, P. Optimal plasticity from matrix memories: what goes up must come down. *Neural Comp.* **2,** 85–93 (1990).
35. Hancock, P. J. B., Smith, L. S. & Phillips, W. A. A biologically supported error-correcting learning rule. *Neural Comp.* **3,** 201–212 (1991).
36. Otto, T., Eichenbaum, H., Wiener, S. I. & Wible, C. G. Learning-related patterns of CA1 spike trains parallel stimulation parameters optimal for inducing hippocampal long-term potentiation. *Hippocampus* **1,** 181–192 (1991).
37. Morrison, B. M., Janssen, W. G. M., Gordon, J. W. & Morrison, J. H. Light and electron microscopic distribution of the AMPA receptor subunit, GluR2, in the spinal cord of control and G86R mutant superoxide dismutase transgenic mice. *J. Comp. Neurol.* **395,** 523–534 (1998).
38. Rayport, S. *et al.* Identified postnatal mesolimbic dopamine neurons in culture: morphology and electrophysiology. *J. Neurosci.* **12,** 4264–4280 (1992).

Acknowledgements. We thank A. J. H. Smith for advice and for the 129 genomic library, J. Ure for embryo injection, L. Anderson and J. Young for mouse care, W. Janssen for technical assistance, F. Johnston and G. Brown for photography, and R. Ellaway for illustrations. This work was supported by the Fyssen Foundation (M.M.) and the BBSRC (M.M., M.D. and P.C.), by grants from the NIH and the Charles A. Dana Foundation (J.H.M. and Y.H.), the Esther A. and Joseph Klingenstein Fund and the Pew Charitable Trusts (T.J.O.), a grant from the National Institute of Mental Health (T.J.O.), and the Wellcome Trust (L.C.W. and S.G.N.G.).

Correspondence and requests for materials should be addressed to S.G.N.G. (e-mail: seth.grant@ed.ac.uk).